Multiaxial Fatigue Strength Assessment of Components Treated by Surface Induction Hardening

T. Palin-Luc[1] , D. Coupard[1], C. Dumas[2] and P. Bristiel[3]

[1] Arts et Métiers ParisTech, Université Bordeaux 1, LAMEFIP, Esplanade des Arts et Métiers, F-33405 Talence Cedex, France, email : thierry.palin-luc@ensam.eu
[2] Renault, Technocentre, DIMAT, TCR LAB 035, 1 Av. du Golf, 78288 Guyancourt Cedex, email : christian.dumas@renault.com
[3]Prisméca, 191 Av. du Général Leclerc, 78220 Viroflay

ABSTRACT. *This paper proposes a method to forecast the fatigue behaviour of parts treated by surface induction hardening (SIH). Surface quenching following surface induction heating is simulated taking into account all the following features of the process: (i) electromagnetic and thermal fields (ii) phase transformation (iii) residual stress field resulting from all the process. The fatigue strength of the specimens was simulated by using Crossland and Dang-Van criteria; the field of the residual stresses, the fatigue characteristics of both the untreated material and the treated layer (martensite) are considered. Fatigue tests on smooth specimens were carried out to compare simulated results with experimental data. These tests inform about the influence of the thermal treatment on the material, including its microstructure evolution and its mechanical characteristics, especially in fatigue. For that purpose, residual stresses were analyzed by X-Ray diffraction before and after the fatigue tests. Fatigue crack initiation areas (at the specimen surface or below) are well predicted depending on the depth of the hardened material layer. The simulation of the fatigue strength at 10^6 ycles is in agreement with experiments.*

INTRODUCTION

Nowadays, the automotive industry needs to reduce the weight and consumption of vehicles for ecological and economical reasons. Thus, the performance of engine components has to be improved to suffer increasing mechanical loads. The development of heat treated parts might answer to this increase of performances to enhance fatigue behaviour. The aim of this article is to present the state of the art on the fatigue characterization of materials treated by induction hardening. Two depths of heat treated material are studied (only one is detailed in this paper due to the limited number of pages) and their properties (metallurgy and residual stresses) are compared to base material properties. A testing fatigue plan was built to evaluate the influence of the depth of heat treated material on the fatigue behaviour. Finally, the simulation of the whole process has been developed and its results compared to measurements. A

methodology to evaluate the multiaxial fatigue strength has been validated. Data obtained in this study are used by engineers to simulate the mechanical behaviour of components and to prevent fatigue failures.

EXPERIMENTS

Based Material and Specimen

This study has been carried out on smooth cylindrical specimens (Figure 1) with a theoretical stress concentration factor of 1.02 in bending [1]. These specimens were machined from round cold-rolled bars of the low alloyed carbon steel D38MnV5S. Three sets of specimens were tested: (a) based material, i.e. untreated specimens with a normalised microstructure, (b) heat treated specimens with an induction hardened depth around 2 mm ("medium depth"), (c) induction heat treated specimens so that the hardening depth was around 3 mm ("large depth").

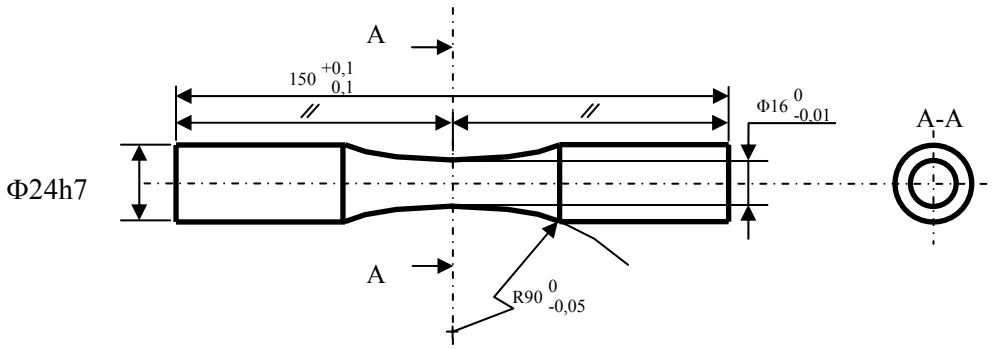

Figure 1. Specimen geometry (Kt=1.02 in bending).

The untreated material has a normalised ferritic-pearlitic microstructure (Figure 2a). Its Vickers hardness is around 300 HV. Some elliptic MnS inclusions surrounded by a short alumina layer were observed (Figure 2b).

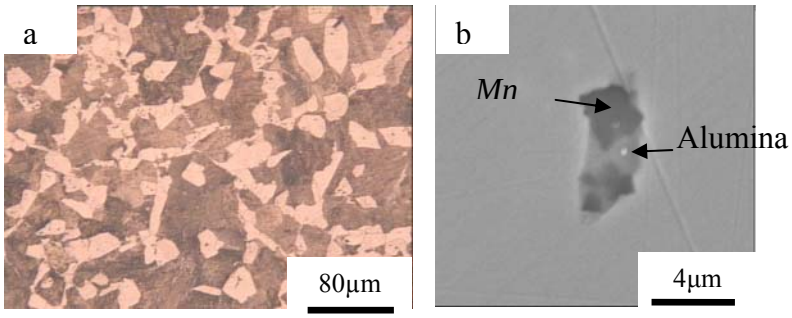

Figure 2. (a) Microstructure of the untreated material, (b) MnS and alumina inclusions.

Induction Process and Heat Treatment

The induction surface treatment was carried out with a 20 kHz induction furnace and a one-turn coil. The heating power was always 190 kW, the total heating time was 1.2 s for the first set of treated specimens (b) and 1.6 s for the second one (c). After the end of the induction heating, the water quenching was started with a delay of 0.5 s. Then, all the treated specimens (sets b and c) were tempered at 180°C during 1h30mn in furnace with inert gas.

Fatigue Tests Conditions

All the fatigue tests were carried out under load control, on a resonant (four points) plane bending fatigue testing machine at a frequency of 50 Hz with the stair-case method, in order to determine the fatigue strength of the specimens at 2.10^6 cycles. For the untreated specimens, the fatigue strength was determined both under fully reversed loading (R=-1) and under constant maximum nominal stress $\sigma_{nom,\max} = 770\ MPa$ (the nominal stress range $\Delta\sigma$ was varying in the stair-case from one specimen to another). For the treated specimens, only the fully reversed fatigue strength in plane bending was determined. Each fatigue strength was determined with 15 specimens (Table 1). The tests were stopped when the resonance frequency decreased more than 2% of the initial frequency (beginning of the fatigue test when the specimen was undamaged). This corresponds to a crack of several millimeters as shown in Figure 3.

Table 1 shows that the fatigue strength at 2.10^6 cycles is magnified by a factor of ~1.3 for the specimens heat treated at a depth of 2 mm and by more than 1.46 for the treatment at large depth (3 mm).

Table 1: Experimental fatigue strength of the specimens at 2.10^6 cycles.

Specimen set	$R = \sigma_{\min} / \sigma_{\max}$	$\Delta\sigma^D_{nom} / 2$ (MPa)
Untreated material (a)	-1	410
Untreated material (a)	R ~ 0.1, $\sigma_{nom,\max} = 770\ MPa$	370
Treated at medium depth (b)	-1	527
Treated at large depth (c)	-1	>600*

(*) The experimental fatigue strength of the specimens treated at large depth (c) is not significant because after the end of the fatigue test, some cracks were observed in the parts of the specimen which are clamped in the machine. This is discussed later. In fact, for these specimens with fatigue crack outside the median torus (testing area), no other crack were observed in the testing area (with diameter of 16 mm). This means that the real fatigue strength for this specimen set is higher than the experimental result of 600 MPa.

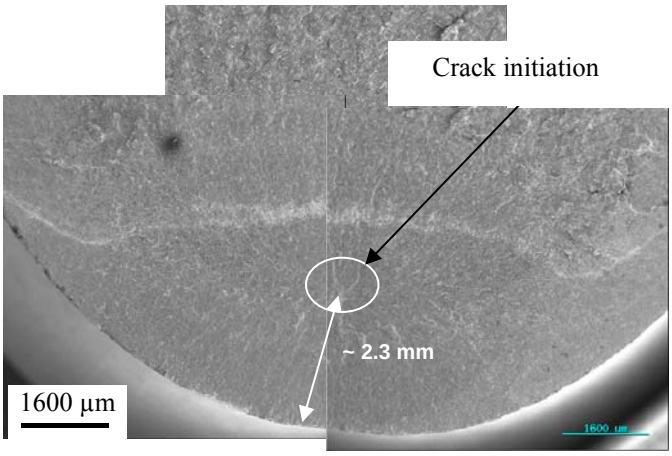

Figure 3. Fracture surface of an induction hardened specimen at medium depth (~2 mm) after plane bending fatigue test at the fatigue strength $\Delta\sigma_{nom}^{D}/2$ =527 MPa.

X-Ray Residual Stress Analysis

Residual stress analysis was conducted by X-Ray Diffraction (XRD) according to the French standard AFNOR XP A 09-285 [2, 3, 4]. The classical "sin2ψ" method has been applied for stress evaluation with the use of at least 11 ψ angles for each stress value. The analysis zone is limited by a collimator of 1 mm in diameter. An " SET - X" XRD apparatus was used which consisted of an X-ray generator; a PC microprocessor; a goniometric head equipped with a ELPHYSE position sensitive detector; a stress analysis software package (SET-X and STERESS-AT) licensed to ENSAM and commercialised by Elphyse and Siemens respectively. XRD have been carried out in martensite or/and ferritic phase with Chromium Kα radiation and {211} plans. The used elastic constants for stress evaluation are: ½ $S_{2\{211\}}$ = 5.83x10^{-6} MPa^{-1}, $S_{1\{211\}}$ = -1.28x10^{-6} MPa^{-1}. The obtained precision on stress analysis is better than 50 MPa which represents a divergence from linearity and comes from a test of the validity of the used method in taking into account of a 35% error in the manipulation of the apparatus. Because of the weak penetration depth of X-ray radiation on specimen (about 5 µm with 66% absorption of incident radiation), the measurements in sub-layer of specimens have been carried out after a local (6mm x 6mm) or circumferential (with 20mm in length) electrolytic polishing (some details are given in [5]). The used solution was a Chlorine based acid electrolyte. The removing speed is about 0.5µm/second under 50 V and 0.5 A.cm^{-2}.

Two material removing techniques were used: local and circumferential electrochemical polishing (at the smallest cross section of the median torus of the specimens). Local material polishing is a fast technique compared to the circumferential material removing

technique. It is known in literature [6] that the XRD results with the local polishing method can be considered as valid when the removal depth is lower than one tenth the diameter for a cylindrical specimen. Beyond this value, the results should be corrected to take into account the stress relaxation resulting from local material removal. According to the authors there is no reliable correction model available for this local removal technique. This means that the only possibility is to use the well-known Moore and Evans correction [6] developed for uniform material removal on a plane specimen. In this case the reliability of the corrected results is doubtful. Circumferential polishing is a quite slow technique, for which a correction model is also needed. In that case, the Moore and Evans model is known to overestimate the correction, which means that the true residual stresses must be considered between the uncorrected and corrected results, especially until one tenth the specimen diameter. For larger depth, the reliability of the correction is not really known. An interesting aspect of the Moore and Evans correction model is to give an estimation of the normal radial stress which can not be directly deduced from experimental analysis. The existence of this normal radial stress below the heat treated specimen surface is undoubtfull with a mechanical point of view, and this is very important for a good estimation of the hydrostatic stress, which is of prior importance in the fatigue crack initiation phenomenon.

SURFACE INDUCTION HARDENING SIMULATION

Modelling of the heat treatment

The finite element software FLUX 2D®, able to solve coupled magneto-thermal problems, has been used to estimate the evolution of the power density and temperature during the induction heating process. This is done by solving the Maxwell's relationships in a stationary state and considering two additional constitutive equations [5]. Solving these relationships enables to determine $\vec{H}$, $\vec{B}$, $\vec{E}$ and $\vec{J}$. The electromagnetic power density dissipated into the workpiece is then given by: $P_e = (\vec{E} \cdot \vec{E}) / \rho_e$. The power density is then integrated directly inside the heat relation through the term $\dot{q}$ in order to estimate the thermal field at each heating step. After heating, FLUX 2D® is used to estimate the spatial and temporal evolution of the temperature during quenching. The heat equation is thus solved by considering (1) a convection boundary limit at the free surface of the sample, (2) an evolution of the material thermal conductivity and specific heat with temperature. At each step of the cooling, the phase and hardness distribution inside the sample are calculated with the software METAL7® from the thermal patterns previously estimated with FLUX2D®. The model is based on the principle of additivity and uses the Johnson-Mehl-Avrami law to estimate the metallurgical transformations and their intensity during cooling from the austenitic temperature until ambient temperature. The thermal and phase distributions during quenching are then injected inside the finite element software MSC

MARC® in order to estimate the residual stress fields. The model needs the mechanical properties of each phase with respect to their temperature of formation and considers that (1) each macroscopic mechanical property obeys a linear mixture law, (2) the material obeys the Von-Mises plasticity criterion, (3) the material mechanical behaviour is thermo-elastic perfectly plastic, (4) the hardening behaviour of the material is isotropic, (5) the total strain tensor is considered as a sum of four tensors: a thermal strain, an elastic strain, a plastic strain, a transformation strain.

Comparison Between Simulation and Experiments

Figures 4 to 6 show the axial, circumferential and radial normal residual stress profiles for specimens hardened at a depth around 2 mm (set b). X-ray analysis was conducted after local electrochemical polishing and the results are presented with and without Moore and Evans correction together with the simulated residual stresses.

As shown in Figures 4 and 5, for both normal stresses, σ_{zz}, and $\sigma_{\theta\theta}$, the residual stress field is compressive over the two first millimetres and then in tension. The maximum compressive stress is quite small in surface, which might result from natural tempering occurring during quenching below MS (martensite starting). The Moore and Evans correction leads to a tensile normal radial residual stress, σ_{rr}, with a maximum value around 150 MPa (Figure 6); this is in very good agreement with the simulation results. This show that the residual stresses are multiaxial below the specimen surface. If the measurement uncertainties are considered, the best agreement between experiments and simulation for σ_{zz} and $\sigma_{\theta\theta}$ is obtained when applying the Moore and Evans correction. In this case, simulated and experimental results are in fairly good agreement until around one tenth the specimen diameter, i.e. 1,6mm.

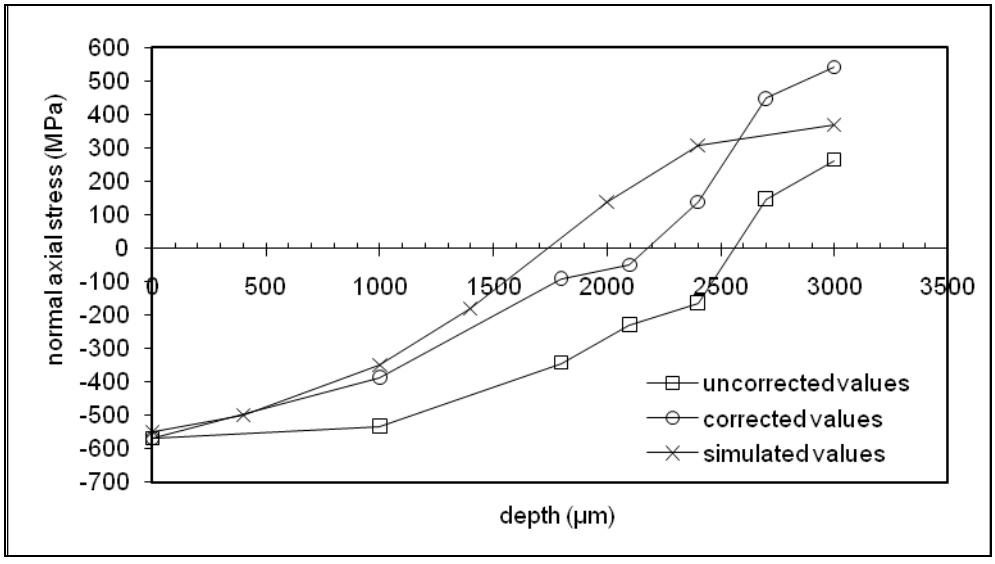

Figure 4. Corrected, uncorrected and simulated normal axial (σ_{zz}) residual stress profiles for an induction treated specimen with a hardening depth ~ 2 mm.

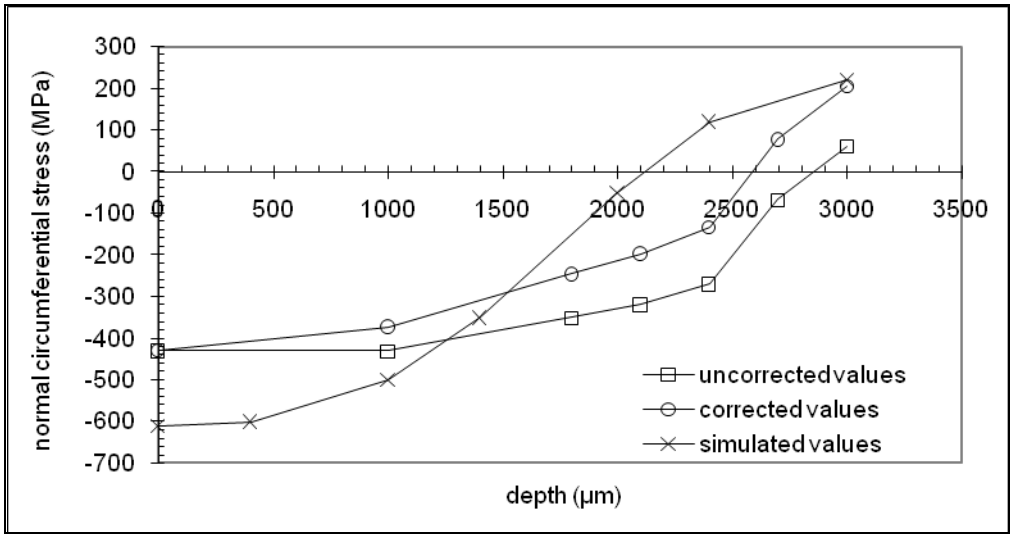

Figure 5. Corrected, uncorrected and simulated normal circumferential ($\sigma_{\theta\theta}$) residual stress profiles for an induction treated specimen with a hardening depth ~ 2 mm.

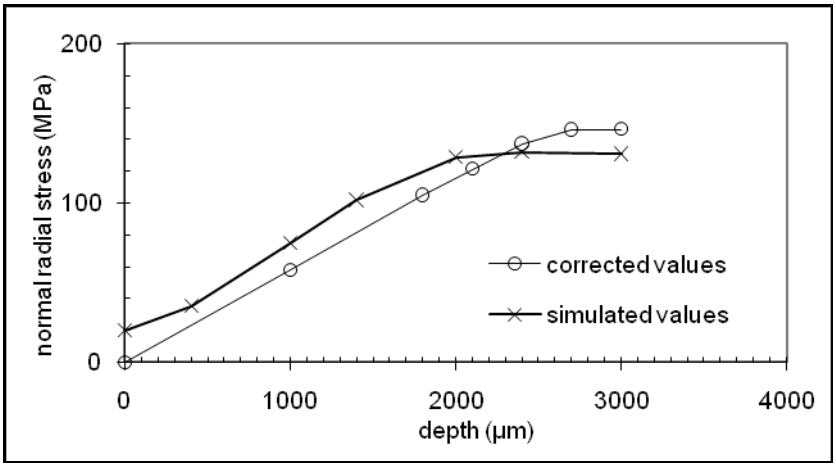

Figure 6. Normal radial (σ_{rr}) residual stress profiles from experimental analysis corrected by Moore/Evans and from simulation.

FATIGUE STRENGTH ASSESSMENT METHOD

Fatigue Strength Modelling

The fatigue strength assessment of specimens treated by surface induction hardening has been done with the following assumptions. (i) The specimens are considered as a two materials structure: the base material and the martensitic heat-treated zone. (ii) The stable residual stresses after relaxation due to cyclic loading are superimposed to the stresses due to the mechanical loading. (iii) Two high cycle multiaxial fatigue criteria

Dang Van [7] and Crossland [9] are assumed to be representative of the fatigue behaviour of the specimens. Both are applied and their results compared hereafter.

At a point M, the Dang Van criterion (1) is depending on the amplitude of the mesoscopic shear stress vector $\left\|\underline{\tau}(M,t,\underline{n})\right\|$ acting on the material plane orientated by the unit normal vector $\underline{n}$ and of the mesoscopic hydrostatic pressure $\sigma_H(M,t)$. The two material parameters α and β can be identified from two fatigue strengths on smooth specimens under different loadings or different stress ratios. In our study, for the based material (a) these parameters were identified from the two fatigue strengths indicated in Table 1.

$$\max_{\underline{n}}\left[\max_{t}\left(\left\|\underline{\tau}(M,t,\underline{n})\right\|+\alpha\sigma_H(M,t)\right)\right]\leq\beta \qquad (1)$$

The Crossland criterion is based on a linear combination of the amplitude of the octahedral shear stress amplitude $\tau_{oct,amp}(M)$ and the maximun hydrostatic stress $\Sigma_{H,\max}(M)$ per load cycle (2). The two material parameters *a* and *b* are identified for the based material from the two fatigue strengths in Table 1.

$$\tau_{oct,a,\Delta J_2}(M)+a\Sigma_{H,\max}(M)\leq b \qquad (2)$$

Due to the high brittleness of the martensite, fatigue tests on full martensitic specimens were impossible. Consequently, the fully reversed fatigue strength under torsion τ^D and plane bending σ^D_{pb} of the martensite were estimated from the maximum compression strength Rm_c of the martensite by using the following empirical relations from CETIM [8]. The fatigue strength in pure rotating bending is related to the maximum tensile strength Rm by: $\sigma^D_{rotbend}\approx R_m(0{,}56-1{,}4.10^{-4}R_m)$. Since the martensite layer in the specimen is in compression due to the residual stresses, the maximum compressive strength has been used whereas the maximum tensile strength. To know this characteristic, quasi-static compression tests were carried out on tubular cylindrical specimens (21 mm long, 13 mm inner diameter, 15 mm outer diameter) machined in the same steel. These specimens were furnace heat treated (180°C – 1h30mm) to get a martensitic tempered microstructure. After tempering, the hardness of the cylindrical specimens was similar to that measured on the fatigue specimens which confirms that natural tempering occurred during the quenching of the specimens after induction surface heating.

Residual Stresses

The stable values of the residual stresses after relaxation (if any) were considered as static stresses superimposed to the stresses due to the cyclic mechanical loading (plane bending in this study). It is very important to note that the complete tensor of residual

stresses is considered in the fatigue strength assessment because of the major role of the hydrostatic stress on the fatigue crack initiation process [9]. Indeed, it has been shown before that the residual stresses are multiaxial.

Comparison Simulation / Experiments

Figure 7 illustrates, for the specimens treated at medium depth (~2mm), the application of the proposed methodology with two criteria (Crossland and Dang Van) at different depth (d in mm) below the specimen surface. This figure shows two families of points. First, the points representative of the cyclic stresses at different depth by considering the experimental residual stresses analysed by XRD. Secondly those from numerical simulation only (points with d underlined). For these simulations the stresses due to cyclic loading were computed with an elastic hypothesis and the residual stresses were computed by finite element analysis of the whole induction process [5].

It is clear in Figure 7, that for the two criteria the proposal does not predict any fatigue crack initiation in the treated material since all the points are below the dashed line representing the fatigue strength of the martensite at 2.10^6 cycles. The difference between Crossland and Dang Van results is not very significant here. But the points representative of depths greater than 2 mm (open symbols) have to be compared with the full line, which corresponds to the threshold of the based material (untreated). It can be seen that in both cases (calculation with experimental residual stresses or with simulated residual stresses), fatigue crack initiation before 2.10^6 cycles should occur at depth between 2.4 and 2.7 mm

This assessment is in very good agreement with the observed crack initiation area on the specimen fracture surface (Figure 3). Such observations were carried out on all the specimens. After the fatigue tests, the specimens were put into liquid nitrogen, then broken by shock to open the natural fatigue crack. The same methodology was used to compute the fatigue strength of the specimens treated at large depth (~3 mm). As previously explained, the experimental fatigue strength in plane bending (R=-1) is unknown but higher than 600 MPa (Table 1). The computed fatigue strength is 670 MPa, and the computed crack initiation area is at the specimen surface. These results are in agreement with experiments.

Discussion

The previous calculations illustrate the high importance of the residual stresses consideration below the surface and the importance to consider their multiaxial character for an accurate high cycle fatigue strength assessment. There are more than 50 fatigue criteria in literature but all of them are not sensitive to the residual stresses (or normal mean stresses). This is not the aim of this paper to detail a lot of fatigue hypothesis. But, for instance the empirical criterion proposed by Gough and Pollard for components under combined bending and torsion is not capable of residual stresses consideration. This is the case of the Von Mises hypothesis too. Whereas, the proposals

made by Papadopoulos [10], Morel [11] should be available for component treated by SIH because they depend on the maximum hydrostatic stress.

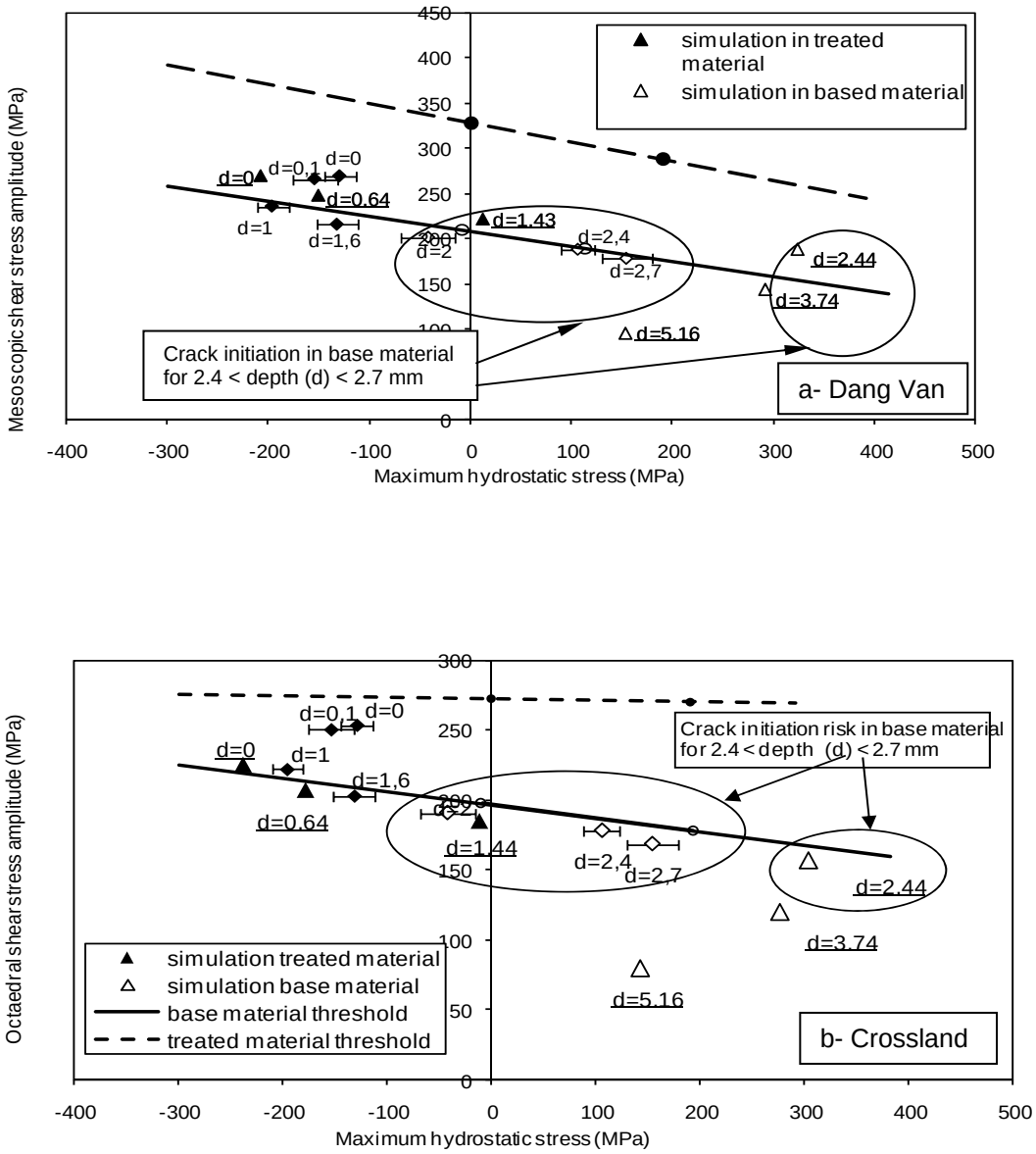

Figure 7. a) Dang Van and b) Crossland diagrammes, for the induction surface hardened specimens at medium depth (~2 mm, set b) with residual stresses both from Xray analysis (◆,◇) and from simulation (▲,△), under fully reversed plane bending at the fatigue strength $\Delta\sigma_{nom}^{D}/2 = 527$ MPa. Horizontal bars illustrate the uncertainty due to XRD analysis uncertainty.

CONCLUSIONS AND PROSPECTS

A global methodology has been developed and validated under plane bending to assess the multiaxial high cycle fatigue strength of a ferritic-pearlitic steel treated by surface induction hardening (SIH). It is assumed that after SIH the specimen is made of two materials (base and treated) with different fatigue properties. Furthermore, it is supposed that residual stresses can be superimposed to the stresses due to the cyclic loading and their mutiaxiality is considered by the hydrostatic stress. It has been shown that considering the residual stress profile all along the radius is very important for an accurate fatigue strength assessment. Indeed, there is a competition between the field of stresses due to the cyclic loading and the residual stresses inside the material. Considering the surface residual stresses is not enough for designing against fatigue crack initiation. Such a proposal gives very good results under fully reversed four points plane bending with both the Crossland and the Dang Van high cycle multiaxial fatigue criteria.

In future, some experiments have to be carried out on martensite. Indeed, a key point of this proposal is the fatigue characterisation of the heat treated material. Furthermore, some investigation should be done under combined proportional and non-proportional loadings (combined bending and torsion for instance) to valid this method under loadings representative of real stress states on components. In this case, other multiaxial fatigue criterion should be tested because of the well-known low accuracy of the Dang Van and the Crossland criteria under non-proportional loadings. Another important aspect for the validation of the proposal is the simulation of residual stresses relaxation. Indeed, in the experiments reported in this paper, since there was no significant residual stress relaxation (experimental observation) the problem was more simple than on any industrial component. Some studies about the simulation of the residual stress relaxation after surface induction hardening have to be done.

REFERENCES

[1] Peterson R.E. (1974) *Stress concentration factors*, Wiley-Interscience publication.
[2] Anon, (1986) X-ray diffraction residual stress techniques, Metal Handbook, ASM, vol. 10.
[3] Prevey P. C. and Mason P. W. (1991) The use of X-ray diffraction to determine the triaxial stress state in cylindrical specimens, Ruud C. Editor, In: Practical applications of residual stress technology), ASM.
[4] Bristiel P., (2001) *Modélisation magnétothermique, métallurgique et mécanique de la trempe superficielle après chauffage par induction appliquée aux vilebrequins*, PhD thesis, ENSAM CER de Bordeaux, France.
[5] Coupard D., Palin-Luc T., Bristiel P., Ji V. and Dumas C. (2009) *Materials Science and Engineering A*, **487**, 328-329

[6] Moore M.G. and Evans W.P., (1958) Mathematical correction for stress in removed layers in X-ray diffraction residual stress analysis. SAE Transactions, Vol. 66, pp. 340-345.
[7] Dang Van K. (1993) In: McDowell DL, Ellis R, editors. *Advances in multiaxial fatigue*, ASTM STP 1191. Philadelphia: ASTM, pp. 120-130.
[8] Brand A., Flavenot J-F., Grégoire R. and Tournier C. (1992) Recueil de données technologiques sur la fatigue, 1992, CETIM, France.
[9] Crossland B. (1956) Effect of large hydrostatic pressures on the torsional fatigue strenght of an alloy steel. Int. Conf. on Fatigue of Metals, London.
[10] Papadopoulos I.V. (1995) *Fatigue Fracture Engng Mat. Structures*, **18**, 79-91.
[11] Morel F. (2001) *Fatigue Fracture Engng Mat. Structures*, **24**, 153-164.